

Analysis of the Impact of Wavelength-Dependent Physical Impairments Considering a Multiband Elastic Optical Network

Ademar Alves dos Santos-Júnior, José Roberto do Nascimento Arcanjo, Helder Alves Pereira and Raul Camelo de Andrade Almeida-Júnior

Abstract—In this paper, we analyze the impact of wavelength-dependent physical impairments, specifically the optical fiber attenuation coefficient (α) and the optical amplifiers noise figure (NF), considering S, C and L bands in a multiband elastic optical network. The calls blocking probability and the distribution of modulation formats among the network accepted calls were used as evaluation metrics. The results obtained for the use of G-652.A optical fiber show that using α and NF with fixed values underestimates the most realistic scenario (α and NF dependent on wavelength). For the use of G-652.D optical fiber, it was possible to obtain a reduction of approximately 63.41% for S band, 95.60% for C band and 98.84% for L band, in terms of calls blocking probability, when the most realistic scenario was compared with the scenario most used in the literature (α and NF with fixed values). In addition, it was verified that, with the most realistic scenario, it was possible to obtain the distribution of more efficient modulation formats using the G-652.D optical fiber in the C band.

Index Terms—Elastic Optical Network, Multiband Transmission, Optical Signal-to-Noise Ratio, Physical Impairment.

I. INTRODUCTION

IN the 1990s, wavelength division multiplexing (WDM) optical networks made it possible to send multiple wavelengths over a single-mode fiber (SMF), in order to expand the data transmission capacity in optical networks [1]. Elastic optical networks (EON) allowed the use of multiple modulation formats and adapted the required bandwidth also according to the transmission bit rate, thus optimizing the usage of frequency spectrum [2]. In this context, space division multiplexing (SDM) optical networks provided great possibilities of using multiple optical fibers, optical fibers with several cores, with several modes and even a combination of different cores and modes in order to increase the capacity of optical networks [3]. However, under certain circumstances, the use of SDM technology can be quite expensive, requiring a greater

number of devices, somewhat increasing capital expenditure and energy consumption [4].

Considering the spectral limitation of C band, the development of new optical amplifiers has allowed the use of other bands for the transmission of optical signals [4]. The use of Erbium-doped fiber amplifiers (EDFA) and amplification systems based on the Raman effect with different configurations (full Raman, Raman plus EDFA or even remotely pumped optical amplifiers) extended the transmission of optical signals to L and S bands, in addition to C band [4].

In the last five years, the concept of optical networks, which use transmission in multiple bands (MB), has gained a lot of attention in the scientific community. Basically, multiband optical networks offer the opportunity to exploit the windows that provide low attenuation values in ITU-T G-652.D SMF optical fibers, expanding the capacity of optical systems by almost 11 times the capacity of C band or nearly 5 times the combined capacity of C and L bands [5]. The great advantage of these optical networks is the high potential, in terms of cost, for eventual upgrades of the optical systems, since they take advantage of the existing infrastructure [5]. It is important to mention that there are already on the market optical systems that use C and L bands, directing research towards data transmission in other bands (O, E and S, for example) [5]. Furthermore, when considering the degradation of the optical signal quality of transmission (QoT), one must take into account the particularities in each of the different transmission bands [6].

In this paper, we extend the work in [7] by analyzing the impact of wavelength-dependent physical impairments, specifically the fiber optic attenuation (α) and the optical amplifiers noise figure (NF), in S, C and L bands, considering three simulation scenarios in a multiband elastic optical network. For our knowledge, no paper, so far, has analyzed the joint impact of different fiber optic attenuation profiles and the noise figure of optical amplifiers as performed in this paper, which is organized as follows: in Section II, the state of the art that refers to papers that analyze the impact of physical impairments in the scenario of multiband optical networks is presented. In Section III, the physical impairments modeling considered in our simulations is described. In Section IV, the parameters, physical topology and simulation scenarios are presented. In Section V, the results obtained are analyzed and, finally, the conclusions are presented in Section VI.

Ademar Alves dos Santos-Júnior, José Roberto do Nascimento Arcanjo and Helder Alves Pereira are with Electrical Engineering Department, Center of Electrical Engineering and Informatics, Federal University of Campina Grande, Campina Grande, Paraíba, Brazil, e-mails: {ademar.santos, jose.arcanjo}@ee.ufcg.edu.br and helder.pereira@dee.ufcg.edu.br.

Raul Camelo de Andrade Almeida-Júnior is with Photonics Groups, Electronics and Systems Department, Center of Technology and Geosciences, Federal University of Pernambuco, Recife, Pernambuco, Brazil, email: raul.almeidajunior@ufpe.br.

The authors of this work would like to thank the State of Paraíba Research Support Foundation (FAPESQ/PB – Grant Term nº 3067/2021) and CNPq for the financial support, and to UFCG and UFPE the institutional support.

Digital Object Identifier: 10.14209/jcis.2023.11.

II. LITERATURE REVIEW

In the literature, it is observed that some authors use analytical expressions to quantify the amplified spontaneous emission (ASE) noise, the stimulated Raman scattering (SRS) effect and the nonlinearities in the receiver nodes [6], [8]–[12], while others use the concept of maximum reach in their works [13]–[16]. The concept of maximum reach is based on the maximum distance at which it is still possible to use a given modulation format. If the distance between the analyzed nodes is greater than a certain threshold, the following modulation format with less spectral efficiency is used to establish the call request.

Regarding the papers that deal with analyzing the impact of the physical impairments in the scenario of multiband optical networks, there are two aspects: (1) those that determine the maximum reach of different modulation formats [13], [17] and (2) those that analyze the impact of different physical impairments on different transmission bands [18]–[23].

Regarding the first aspect, Paz *et al.* [13] study the effect that linear and nonlinear noise accumulation in multiband optical systems has on the transmission reach for optical signals managed by an EON operator. Using fiber propagation models they estimate the maximum transmission reach for a variety of modulation formats commonly used in EONs for each transmission band in a multiband network scenario. The authors consider ASE noise and nonlinearities in their analysis, optical SMF fiber, fixed values of noise factor and attenuation coefficient, in addition to using E, S, C and L bands. The results obtained involve maximum reach for a variety of modulation formats (BPSK, QPSK, 16-QAM, 64-QAM and 256-QAM) with three commonly used threshold values in EONs. Uzunidis *et al.* [17] tabulate the state of the art details for commercially and experimentally available optical components, and discuss their specifications and their impact on the overall system performance. The authors employ a novel physical layer formalism, which calculates the performance of a multiband transmission system considering an amplification scheme based on commercially available rare-earth doped fiber amplifiers for S, C and L bands. This formalism considers ASE noise, four wave mixing (FWM) and SRS as physical impairments. Finally, they calculate the attainable capacity and maximum reach for each band and for three different modulation formats (QPSK, 16-QAM and 64-QAM). In their analysis, the authors consider the attenuation coefficient value to be constant.

Regarding the second aspect, Cantono *et al.* [18] review the generalized Gaussian noise (GGN) model for multiband prediction of nonlinear interference (NLI) generation and validate its accuracy by comparing C+L simulative results to model predictions. Results are obtained for the case of amplification using a hybrid Raman and Erbium-doped fiber amplifiers. The authors consider ASE noise and nonlinearities as physical impairments, C and L bands and a WDM optical system. Furthermore, the attenuation coefficient value is modeled as an analytical function for the analyzed bands. Ferrari *et al.* [19] calculate the maximum transmission capacity for G-652.D optical fiber, considering three different fiber span

lengths for a WDM optical system involving the L, C, S, E and O bands. The GGN model is used for consideration of physical impairments but the values of the noise figures of the amplifiers are constant in the simulations. D'Amico *et al.* [20] investigate the main features of the C+L implementation from an operational point of view, considering the generalized signal-to-noise-ratio (GSNR) as the system metric. The authors focus their analysis on the leading contributors to the GSNR degradation in a C+L scenario, highlighting the main mutual inter-band interactions that have to be considered in order to set the system working point to a level that provides the best possible system performance. They consider wavelength-varying attenuation and noise figure, SRS nonlinear interference as physical impairments, and G-652.D optical fiber. Nikolaou *et al.* [21] study the physical layer performance in a WDM optical system which exploits O, E, S, C and L bands. The authors consider ASE noise, nonlinear interference and SRS effect as physical impairments. In their simulations, they consider fixed values of attenuation coefficient and noise figure for each band. D'Amico *et al.* [22] investigate the quality of transmission estimation in a multiband transmission scenario, including a wideband description of the frequency-dependent physical layer parameters and a disaggregated QoT estimation approach. The authors use experimentally-derived Erbium- and Thulium-doped fiber amplifier operational data, and simulate the generation of the nonlinear interference noise by comparing implementations of the split-step Fourier method, the GGN model implemented in an open-source library, and an efficient approximation that provides accurate results in a limited computational time. The authors consider ASE noise and NLI as physical impairments, frequency-dependent evolution of the fiber loss, G-652.D optical fiber and analyze the results in a WDM optical system. Gomes *et al.* [23] analyze the node components and architectures for the C+L band, and their cost and power consumption are estimated. The impact of ASE noise and NLI on the optical signal-to-noise ratio (OSNR) of the horseshoe topology is studied for filterless L band amplified solutions and the influence of in-band crosstalk on the electrical signal-to-noise ratio (SNR) is considered for unamplified solutions. They consider fixed values of attenuation coefficient and noise figure, in addition to considering ASE noise and nonlinearities as physical impairments. As can be seen, the objective of these papers [18]–[23] was not to exclusively analyze the performance of multiband optical networks in relation to the dependence of physical impairments on wavelength. According to the state of the art, no paper, so far, has analyzed the joint impact of different fiber optic attenuation profiles and the noise figure of optical amplifiers in a MB-EON scenario as performed in this paper. Table I presents the state of the art with regard to papers dealing with the analysis of the impact of physical impairments in the context of multiband optical networks.

III. PHYSICAL IMPAIRMENTS MODELING

In this paper, we considered a node architecture adapted to MB scenario and based on spectral switching architecture [24], as shown in Fig. 1.

Table I: State of the art with regard to papers dealing with the analysis of the impact of physical impairments in the context of multiband optical networks.

Reference	Optical Network	Optical Fiber	O band	E band	S band	C band	L band	U band	ASE	SRS	SPM	XPM	NLI
[18]	WDM	–	–	–	–	X	X	–	X	–	–	–	X
[19]	WDM	G.652D	X	X	X	X	X	–	X	X	–	–	X
[20]	WDM	G.652D	–	–	–	X	X	–	X	X	X	X	X
[21]	WDM	SMF	X	X	X	X	X	–	X	X	–	–	X
[22]	WDM	G.652D	–	–	X	X	X	–	X	X	X	X	X
[23]	WDM	–	–	–	–	X	X	–	X	–	X	X	X

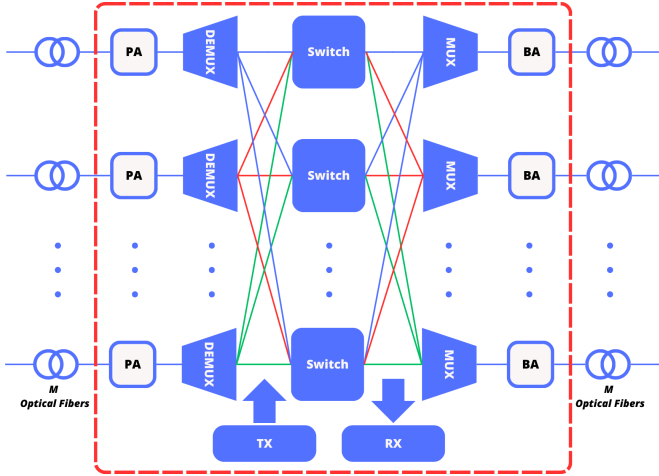


Figure 1: Node architecture adapted to MB scenario and based on spectral switching architecture [24].

This node architecture jointly with the link configuration, in terms of spans, have the following devices: transmitter (TX), switch, multiplexer (MUX), booster optical amplifier (BA), optical fiber, in-line optical amplifier, pre-amplifier (PA), demultiplexer (DEMUX) and receiver (RX), as shown in Fig. 2.

In this paper, we considered that the booster optical amplifiers and pre-amplifiers, present in the nodes, and the in-line optical amplifiers, present along the links, exactly compensate the node and link losses. Thus, the optical signal-to-noise ratio obtained at the destination node ($OSNR_{out}$) can be evaluated considering the values of the losses and gains in the devices, and the ASE noise generated in the optical amplifiers such as

$$OSNR_{out} = \frac{P_{in}}{N_{in} + N_{AMP}}, \quad (1)$$

in which P_{in} represents the input optical power per slot, N_{in} the transmitter noise power and N_{AMP} the total noise power generated by the optical amplifiers.

Basically, the ASE noise power generated in EDFAs for both polarizations of electromagnetic wave can be evaluated as [25]

$$N_{EDFA} = h \cdot \nu \cdot F \cdot B_{Ref} \cdot (G - 1), \quad (2)$$

in which h represents the Planck constant, ν the optical frequency of the first slot of the call request, F the optical amplifier noise factor, B_{Ref} the reference bandwidth and G the linear gain of the optical amplifier. As can be seen in Eq. (2), N_{EDFA} directly depends on the noise factor and the gain of

the optical amplifier. However, depending on the amount and the types of optical amplifiers used, in addition to the devices present along a lightpath, it is possible that the total noise power generated by the optical amplifiers depends on several factors. For a lightpath with l links, N_{AMP} is evaluated as

$$N_{AMP} = N_{BA} + N_{AL} + N_{PA}, \quad (3)$$

in which N_{BA} represents the total ASE noise power generated by the booster optical amplifiers, N_{AL} the total ASE noise power generated by the in-line optical amplifiers and N_{PA} the total ASE noise power generated by the pre-amplifiers. These parameters can be calculated by the following equations (Eq. (4) to (6)), considering the node and link architecture illustrated in Fig. 2:

$$N_{BA} = h \cdot \nu \cdot F \cdot B_{Ref} \cdot \frac{l \cdot (L_{Sw} \cdot L_{Mx}^2 \cdot L_{Dx} - 1)}{L_{Mx}}, \quad (4)$$

$$N_{AL} = h \cdot \nu \cdot F \cdot B_{Ref} \cdot \sum_{i=1}^l \left[\frac{s_i}{L_{Mx}} \cdot (L_{Mx} \cdot L_{Dx} \cdot L_{Fbi}^{1/(s_i+1)} - 1) \right] \quad (5)$$

and

$$N_{PA} = h \cdot \nu \cdot F \cdot B_{Ref} \cdot \sum_{i=1}^l \left[\frac{L_{Mx} \cdot L_{Dx}^2 \cdot L_{Sw} \cdot L_{Fbi}^{1/(s_i+1)} - 1}{L_{Mx} \cdot L_{Dx} \cdot L_{Sw}} \right], \quad (6)$$

in which L_{Sw} represents the linear switch loss, L_{Mx} the linear multiplexer loss, L_{Dx} the linear demultiplexer loss, L_{Fbi} the linear optical fiber loss corresponding to the i -th link and s_i the number of in-line optical amplifiers belonging to the i -th link and evaluated as

$$s_i = \left\lceil \frac{d_{ij}}{d_{amp}} - 1 \right\rceil, \quad (7)$$

in which $\lceil u \rceil$ represents the smallest integer not less than u , d_{ij} the physical length of the link ij and d_{amp} the span length.

Fig. 3 shows the attenuation coefficient ($\alpha(\lambda)$), in dB/km, for two types of optical fiber (G652.A and G652.D) (left axis) [26], as well as the noise figure ($NF(\lambda)$), in dB, of specific optical amplifiers (right axis), both depending on the wavelength, considering: (a) S band [27]; (b) C band [22] and (c) L band [28]. The dependence of these two parameters on the wavelength was modeled according to data available in the literature [22], [26]–[28].

The threshold optical signal-to-noise ratio ($OSNR_{th}$), depending on transmission bit rate, modulation format and

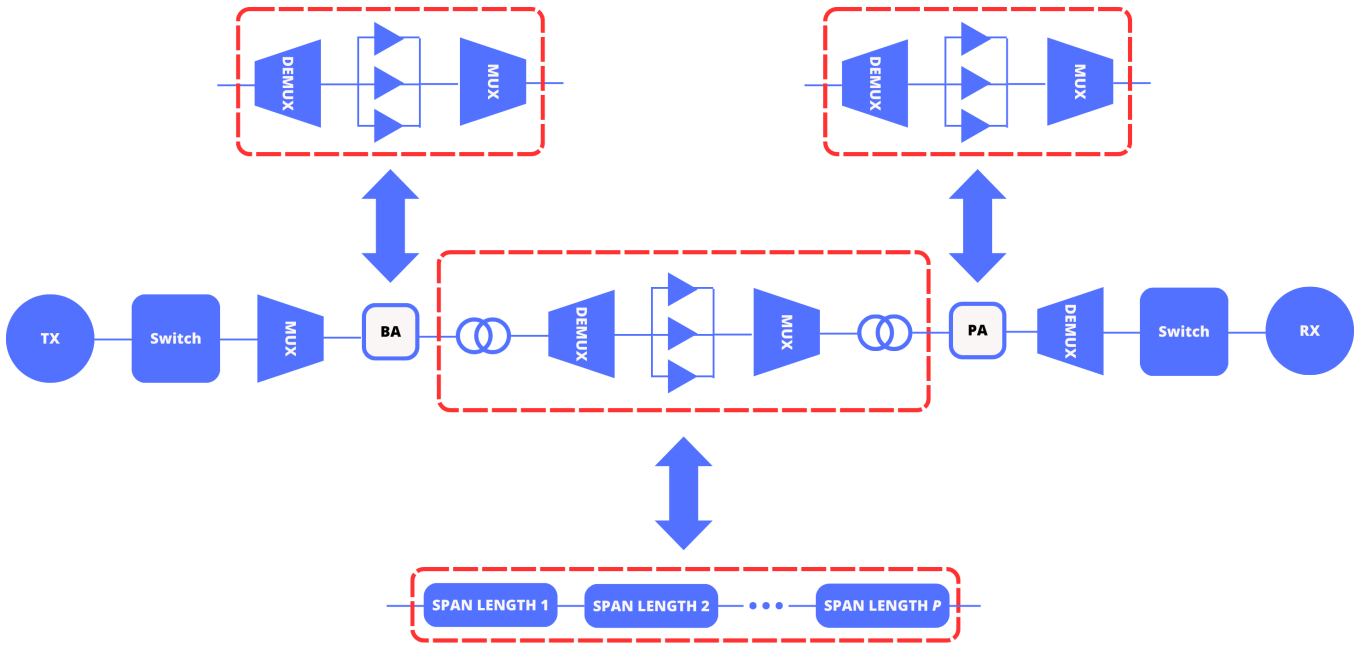


Figure 2: Devices present along an optical link.

signal-to-noise ratio per bit (snr_b), can be used as a QoT evaluation parameter of the call request, in comparison with the value obtained from the $OSNR_{out}$ [29]. Assuming a maximum tolerable bit error rate of 10^{-3} and using a forward error correction (FEC) code, for modulation format 4-QAM, one has to $snr_b = 6.79$ dB, 8-QAM, $snr_b = 8.58$ dB, 16-QAM, $snr_b = 10.52$ dB, 32-QAM, $snr_b = 12.59$ dB, and 64-QAM, $snr_b = 14.77$ dB [30]. Thus, for a given transmission bit rate and a respective modulation format, the $OSNR_{th}$ can be evaluated as [30]

$$OSNR_{th} = \frac{1}{2} \frac{B}{B_{Ref}} snr_b, \quad (8)$$

in which B represents the transmission bit rate and B_{Ref} the reference bandwidth.

The number of slots for a given call request (n_{slot}) can be evaluated as [30]

$$n_{slot} = \left\lceil \frac{B}{2B_{Slot} \log_2 M} \right\rceil, \quad (9)$$

in which B_{Slot} represents the slot bandwidth and M the number of symbols for an M -QAM modulation format.

IV. SIMULATION SETUP

The simulations carried out in this paper used the NSFNet topology, as shown in Fig. 4, and the parameters described in Table II [7] and Table III [31].

Three simulation scenarios were analyzed ($CS1$, $CS2$ and $CS3$). $CS1$ considered the network performance in which both α and NF have fixed values. $CS2$ considered the performance of the network in which α and/or NF can be dependent on the wavelength, considering the transmission in G652.A optical fiber. $CS3$ considered the same aspects as $CS2$, however, the G652.D optical fiber was used. For performance analysis, we

Table II: Parameters used in our simulations [7].

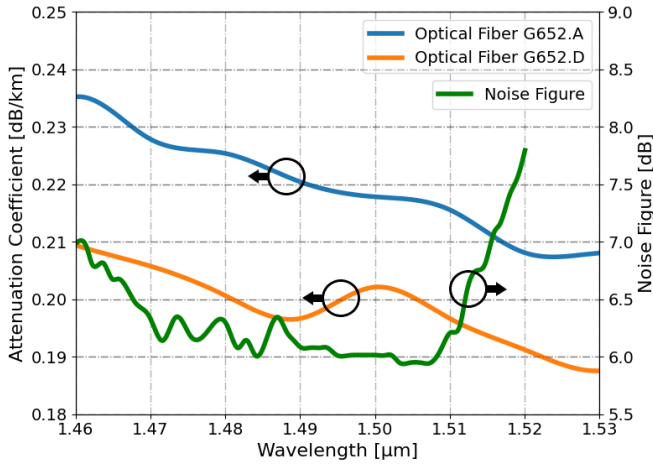
Parameter	Value
Span length	70 km
Modulation formats	4, 8, 16, 32 and 64-QAM
Reference bandwidth	12.5 GHz
Slot bandwidth	12.5 GHz
Input optical signal-to-noise ratio	30 dB
Transmission bit rates	From 100 to 500 Gbps with uniform distribution

Table III: Simulation parameters for S, C and L bands [31].

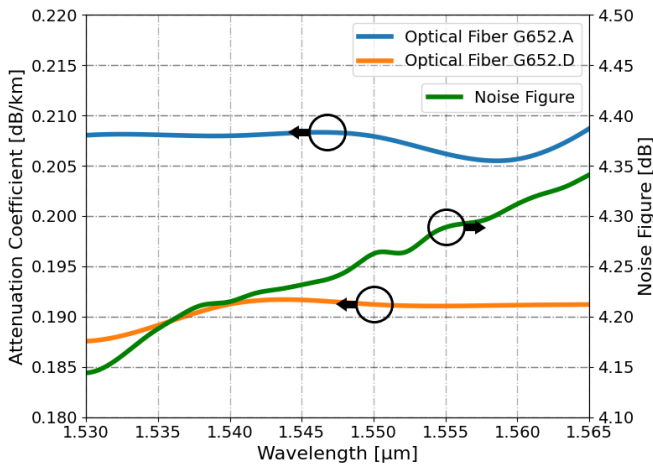
Parameter	S band	C band	L band
Initial wavelength (nm)	1460.00	1530.37	1571.26
Final wavelength (nm)	1521.16	1565.03	1614.41
Initial frequency (THz)	197.22	191.69	185.83
Final frequency (THz)	205.48	196.03	190.93
Total number of slots	661	347	408
Noise figure (dB)	7.0	5.5	6.0
Attenuation coefficient (dB/km)	0.220	0.191	0.200

considered the calls blocking probability (PB) as a function of the network load and the distribution of modulation formats among the network accepted calls.

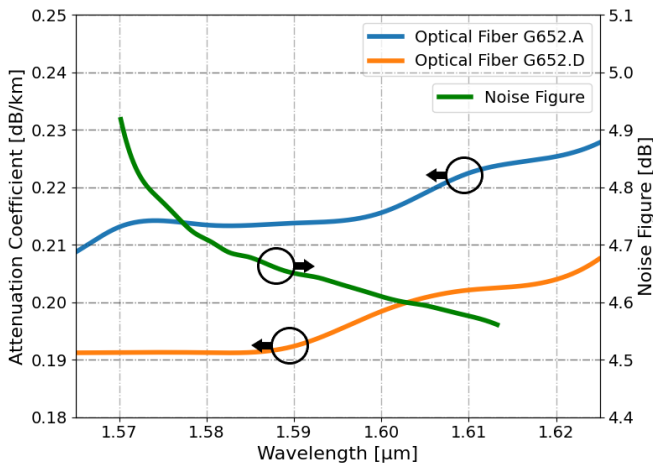
We adopted the following methodology to define the network load range and the input optical power per slot (P_{in}) for each band considered in our simulations: (1) several simulations were carried out with different network load values considering PB as a function of P_{in} ; (2) the lowest network load limit was defined as the first one that reached $PB = 10^{-3}$ considering $0 \leq P_{in} \leq 5$ dBm; (3) the P_{in} value for the lowest network load limit was selected as the optimal value of the respective band; (4) the upper network load limit was defined as the first one that reached $PB = 10^{-1}$ considering $5 \leq P_{in} \leq 10$ dBm. With this, we obtained the following network load ranges for the respective bands: (1) 1200 to 2300 Erlangs with $P_{in} = 2$ dBm for S band; (2) 500 to 1050 Erlangs with $P_{in} = 0$ dBm for C band; and (3) 600 to



(a) S band.



(b) C band.



(c) L band.

Figure 3: Attenuation coefficient ($\alpha(\lambda)$), in dB/km, for two types of optical fiber (G652.A and G652.D) (left axis) [26], as well as the noise figure ($NF(\lambda)$), in dB, of specific optical amplifiers (right axis), both depending on the wavelength, considering: (a) S band [27]; (b) C band [22] and (c) L band [28].

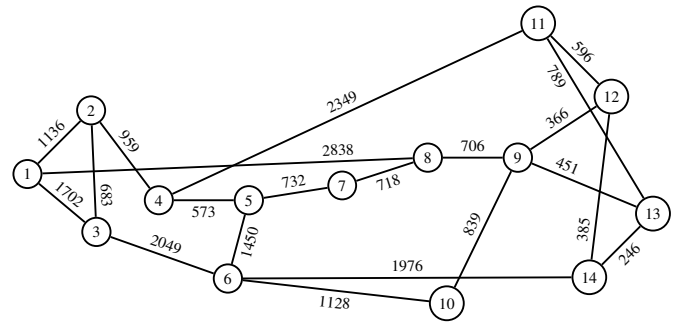


Figure 4: NSFNet topology.

1150 Erlangs with $P_{in} = 0$ dBm for L band, as shown in Fig. 5.

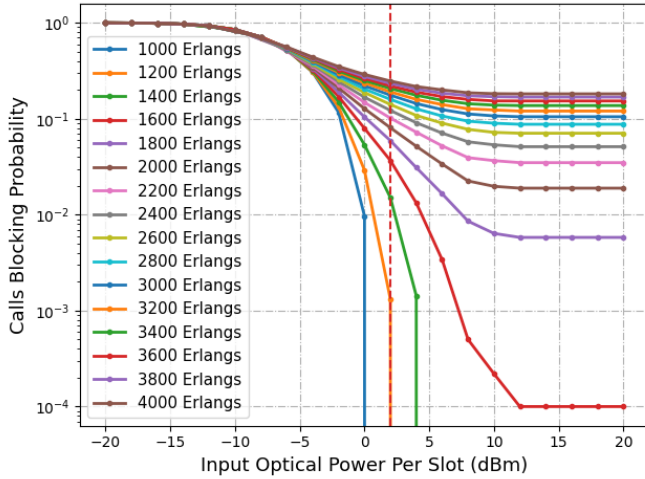
To carry out the simulations, an open source computational platform (SONDA) available in the literature [32], [33] was used. SONDA is capable of handling WDM/EON optical network scenarios in dynamic traffic situations. At the moment, it is also able to tackle with routing and resource assignment problems in SDM and MB optical networks, considering physical impairments such as ASE noise, in both technologies, and intercore and intracore crosstalks in the first (SDM).

For a given call request to be established, the following steps need to be met: (1) there must be a route between the source and destination nodes; (2) there must be available spectral resources along this route; and (3) the $OSNR_{out}$ must be above a pre-established threshold ($OSNR_{th}$). If any of these criteria cannot be attended, the call request is blocked. The process is repeated until the number of calls, or the number of blockings, provided by the user is reached. The route between the source and destination nodes is obtained using the shortest path algorithm, considering physical distance. For a call request, modulation formats are assigned in order of the most efficient ones. When it is not possible, the next most efficient is tried until the last attempt is made with the 4-QAM modulation format. For the spectrum assignment step, the First-Fit algorithm is used.

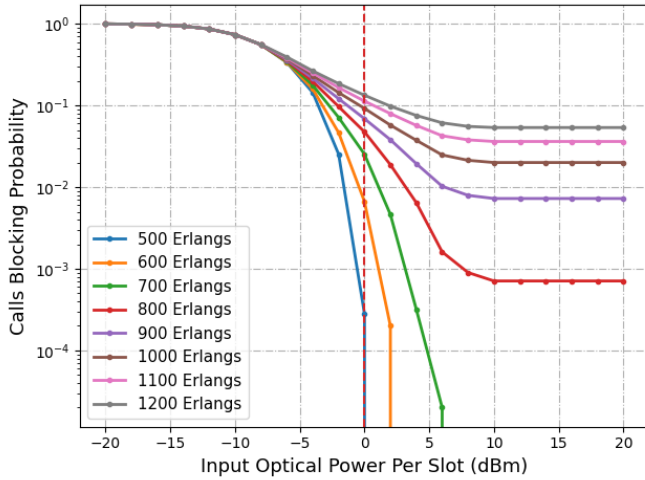
All simulations were performed considering dynamic traffic. The following parameters were considered: (1) 100 blockings for analysis of calls blocking probability, (2) 10^4 call requests and (3) 1200 Erlangs for S band, 500 Erlangs for C band and 600 Erlangs for L band when it is considered the analysis of distribution among the assigned modulation formats to the network accepted calls.

V. RESULTS

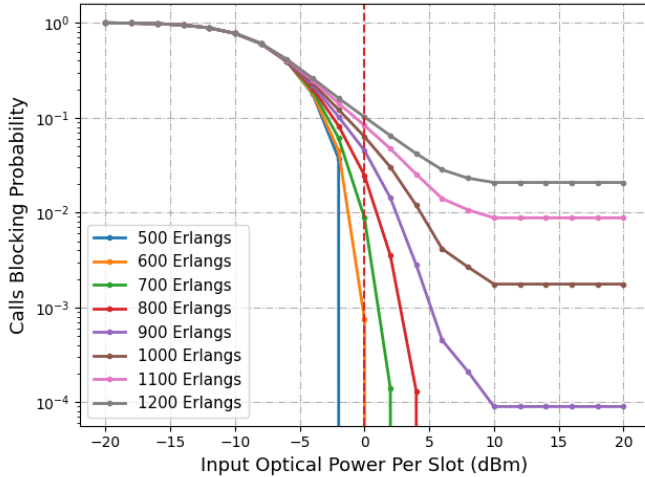
Fig. 6 shows the calls blocking probability as a function of the network load, considering three scenarios for α and NF for each transmission band (S, C and L): (1) α and NF with fixed values ($CS1$) (Fig. 6a, Fig. 6d and Fig. 6g), (b) α with fixed value, or depending on the wavelength, in combination with NF with fixed value, or depending on the wavelength, using G652.A optical fiber ($CS2$) (Fig. 6b, Fig. 6e and Fig. 6h) and (3) α with fixed value, or depending on the wavelength, in combination with NF with fixed value, or depending on the wavelength, using G652.D optical fiber ($CS3$) (Fig. 6c, Fig. 6f and Fig. 6i).



(a) S band.



(b) C band.



(c) L band.

Figure 5: Methodology based on calls blocking probability to define the network load range and the input optical power per slot to our simulations for: (a) S band, (b) C band and (c) L band.

For CS1 scenario (Fig. 6a, Fig. 6d and Fig. 6g), one can note that the lower is α , the lower is the calls blocking probability. This is due to the fact that the total ASE noise power generated in in-line optical amplifiers (Eq. (5)) and in pre-amplifiers (Eq. (6)) directly depends on the linear optical fiber loss (L_{FB}). Thus, the greater is the attenuation value (α), the greater is the value of the total ASE noise power (N_{AMP}) (Eq. (3)), which reduces the value of $OSNR_{out}$ (Eq. (1)), requiring modulation formats with lower spectral efficiency and, consequently, additional slots for light-path establishments. Table IV presents the results of CS1 scenario, in terms of calls blocking probability, considering the network load value equal to 1200 Erlangs for S band, 500 Erlangs for C band and 600 Erlangs for L band.

For CS2 scenario, in which the G652.A optical fiber is used for the transmission of optical signals, it can be seen that, for S band (Fig. 6b), the best performance in terms of calls blocking probability is obtained with $\alpha = 0.220$ dB/km and $NF(\lambda)$. It is important to point out that the total ASE noise power generated by the in-line optical amplifiers and pre-amplifiers depends directly on the amplifier noise factor (F) and the linear optical fiber loss (L_{FB}) (Eq. (5) and Eq. (6)). Thus, the smaller the $F \cdot L_{FB}$ product, the better the performance in terms of calls blocking probability. However, a more realistic scenario, involving $\alpha(\lambda)$ and $NF(\lambda)$, results in a worse performance due to the fact that the average value of α ($\bar{\alpha}_S = 0.2216$ dB/km) for S band is above of α fixed value used in the simulations ($\alpha = 0.220$ dB/km). The small difference when comparing the simulations performed with NF fixed value ($NF = 7.0$ dB) and $NF(\lambda)$ is due to the slight difference between the average value of NF ($\bar{NF}_S = 6.5246$ dB) and the NF fixed value used in the simulations ($NF = 7.0$ dB). In the case of C band (Fig. 6e), it is plausible to consider both α and NF with fixed values ($\alpha = 0.191$ dB/km and $NF = 5.5$ dB), resulting in a good approximation with the more realistic scenario ($\alpha(\lambda)$ and $NF(\lambda)$). However, due to the fact that the average value of α ($\bar{\alpha}_C = 0.2074$ dB/km) is above of the α with fixed value ($\alpha = 0.191$ dB/km) considered for this band, the worst performance is obtained with $\alpha(\lambda)$ and $NF = 5.5$ dB configuration. For L band (Fig. 6h), the behavior is very similar to that of C band (Fig. 6e), so that the best performance obtained by the α with fixed value ($\alpha = 0.200$ dB/km) and $NF(\lambda)$ configuration underestimates the more realistic scenario ($\alpha(\lambda)$ and $NF(\lambda)$). The difference between the results in terms of calls blocking probability of the curves considering NF with fixed value and $NF(\lambda)$ is due to the fact that the average value of NF is below of the value considered fixed for both transmission bands ($\bar{NF}_C = 4.2489$ dB $<$ 5.5 dB for C band and $\bar{NF}_L = 4.6656$ dB $<$ 6.0 dB for L band). Table V presents the results of CS2 scenario, in terms of calls blocking probability, considering the network load value equal to 1200 Erlangs for S band, 500 Erlangs for C band and 600 Erlangs for L band.

For CS3 scenario, in which the G652.D optical fiber is used for the transmission of optical signals, it can be seen that, for S band (Fig. 6c), the configurations that considered $\alpha(\lambda)$ resulted in the best performance in terms of calls blocking probability. This can be explained by the fact that the average

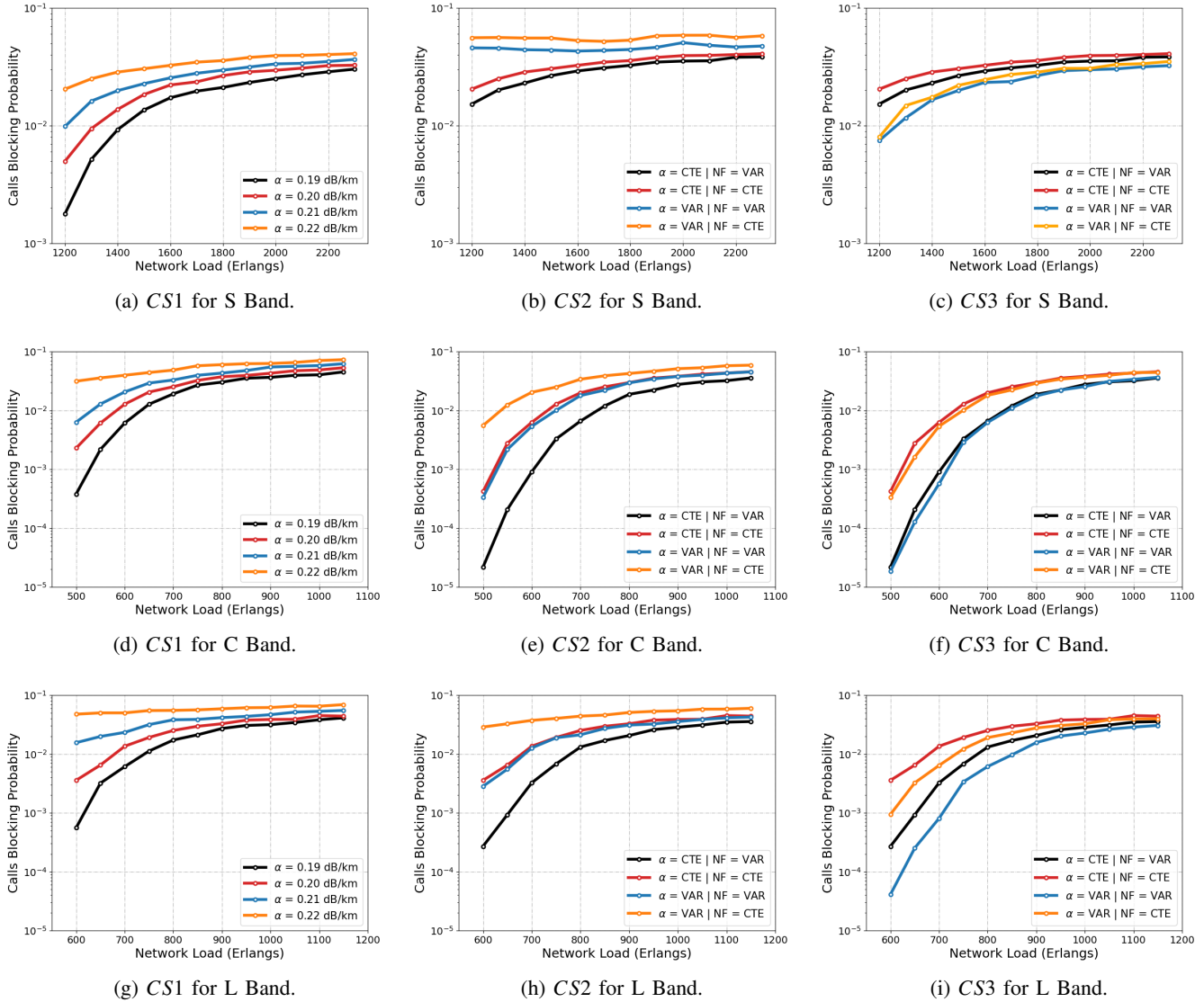


Figure 6: Calls blocking probability as a function of the network load, considering three scenarios for α and NF for each transmission band (S, C and L): (1) α and NF with fixed values (CS1) (Fig. 6a, Fig. 6d and Fig. 6g), (b) α with fixed value, or depending on the wavelength, in combination with NF with fixed value, or depending on the wavelength, using G652.A optical fiber (CS2) (Fig. 6b, Fig. 6e and Fig. 6h) and (3) α with fixed value, or depending on the wavelength, in combination with NF with fixed value, or depending on the wavelength, using G652.D optical fiber (CS3) (Fig. 6c, Fig. 6f and Fig. 6i).

Table IV: Results of CS1 scenario, in terms of calls blocking probability, considering the network load value equal to 1200Erlangs for S band, 500Erlangs for C band and 600Erlangs for L band.

α (dB/km)	S band		C band		L band	
	NF (dB)	PB	NF (dB)	PB	NF (dB)	PB
0.19	7.0	1.79×10^{-3}	5.5	3.80×10^{-4}	6.0	5.58×10^{-4}
0.20	7.0	4.99×10^{-3}	5.5	2.29×10^{-3}	6.0	3.57×10^{-3}
0.21	7.0	9.85×10^{-3}	5.5	6.32×10^{-3}	6.0	1.56×10^{-2}
0.22	7.0	2.04×10^{-2}	5.5	3.13×10^{-2}	6.0	4.75×10^{-2}

value of α ($\bar{\alpha}_S = 0.2004$ dB/km) is below of the α with fixed value considered in the simulations ($\alpha = 0.220$ dB/km),

Table V: Results of CS2 scenario, in terms of calls blocking probability, considering the network load value equal to 1200 Erlangs for S band, 500 Erlangs for C band and 600 Erlangs for L band.

α (dB/km)	S band		α (dB/km)	C band		α (dB/km)	L band	
	NF (dB)	PB		NF (dB)	PB		NF (dB)	PB
0.220	7.0	2.04×10^{-2}	0.191	5.5	4.21×10^{-4}	0.200	6.0	3.57×10^{-3}
0.220	$NF(\lambda)$	1.53×10^{-2}	0.191	$NF(\lambda)$	2.18×10^{-5}	0.200	$NF(\lambda)$	2.71×10^{-4}
$\alpha(\lambda)$	$NF(\lambda)$	4.58×10^{-2}	$\alpha(\lambda)$	$NF(\lambda)$	3.32×10^{-4}	$\alpha(\lambda)$	$NF(\lambda)$	2.83×10^{-3}
$\alpha(\lambda)$	7.0	5.58×10^{-2}	$\alpha(\lambda)$	5.5	5.53×10^{-3}	$\alpha(\lambda)$	6.0	2.87×10^{-2}

resulting in a smaller amount of total ASE noise power at the receiver node and resulting in a smaller calls blocking probability due to the lack of QoT. In this case, configurations that assumed α with fixed value resulted in poor calls blocking probability performance. Although the average value of NF for this band be 6.5246 dB (\overline{NF}_S), the difference between considering fixed or wavelength dependent value for NF did not compromise the result obtained when it is considered the $F \cdot L_{Fb}$ product. The performance of the most realistic scenario, compared to the scenario most used in the literature (α and NF with fixed values) [21], [23], resulted in a reduction of approximately 63.41% in terms of calls blocking probability. For C band (Fig. 6f), it was possible to observe that the most realistic scenario obtained the best results compared to those obtained when α and NF had fixed values, scenarios used in the literature in the majority of the cases [21], [23]. It was verified that this is due to the fact that the average value of α ($\overline{\alpha}_C = 0.1907$ dB/km) was below that with fixed value considered in the simulations ($\alpha = 0.191$ dB/km) and that the average value of NF ($\overline{NF}_C = 4.2489$ dB) was below the considered fixed value of NF (5.5 dB) in the simulations, contributing to these results. As a result, the most realistic scenario resulted in calls blocking probability reduction of approximately 95.60% compared to the scenario with fixed parameters used in the literature [21], [23]. For L band (Fig. 6i), a behavior similar to that obtained for C band was observed, in which the most realistic scenario performed with calls blocking probability reduction of approximately 98.84% lower when compared to the constant parameters scenario used in the literature [21], [23]. Table VI presents the results of CS3 scenario, in terms of calls blocking probability, considering the network load value equal to 1200 Erlangs for S band, 500 Erlangs for C band and 600 Erlangs for L band.

Fig. 7 (Fig. 8 and Fig. 9) shows the distribution of assigned modulation formats to the network accepted calls, considering S (C and L) band, a network load value equal to 1300 Erlangs (700 and 800 Erlangs) and different scenarios for α and NF .

It can be seen that, in the scenario referring to the fixed values of α and NF (Fig. 7a to Fig. 7d, Fig. 8a to Fig. 8d and Fig. 9a to Fig. 9d), the lower α value, the lower the total ASE noise power generated in the network, which improves the $OSNR_{out}$ and enables the acceptance of more call requests with more efficient modulation formats in spectral terms. In this way, the call requests accepted by the network start to be distributed in a more accentuated way for the more efficient

modulation formats along the decrease of the value of α used in the simulations.

When using G652.A optical fiber, the average value of α is approximately 0.2216 dB/km for S band (0.2074 dB/km for C band and 0.2157 dB/km for L band). When using G652.D optical fiber, the average value of α is approximately 0.2004 dB/km for S band (0.1907 dB/km for C band and 0.1952 dB/km for L band). The average value of NF is approximately 6.5246 dB for S band (4.2489 dB for C band and 4.6656 dB for L band). As the total ASE noise power directly depends on the linear optical fiber loss and the noise factor (Eq. (5) and Eq. (6)), the smaller the product of these two parameters, more call requests can be accepted with more efficient modulation formats. This behavior is observed when comparing the distribution of modulation formats between Fig. 7e and Fig. 7f for S band (Fig. 8e and Fig. 8f for C band and Fig. 9e and Fig. 9f for L band). It can be seen that a more accentuated concentration of accepted call requests in more efficient modulation formats is observed in the G652.D optical fiber, since the QoT degradation is smaller. The results shown in Fig. 8f for C band present the better usability of more efficient modulation formats, culminating in the best utilization values of all scenarios evaluated in this paper (0.00% for 4-QAM, 5.04% for 8-QAM, 20.97% for 16-QAM, 30.15% for 32-QAM, and 43.84% for 64-QAM). Table VII (Table VIII and Table IX) presents the distribution, in terms of percentage, of assigned modulation formats to the network accepted calls, considering a network load value equal to 1200 Erlangs in S band (500 Erlangs in C band and 600 Erlangs in L band).

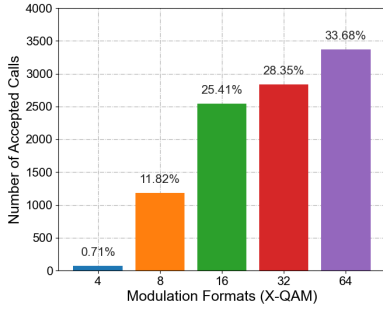
Considering CS3 for C band, $\alpha_{G652.D}(\lambda)$ and $NF(\lambda)$, we obtained an average calls blocking probability of 1.85×10^{-5} with a margin of error of 8.45×10^{-7} , corresponding to confidence intervals of 99%, for 30 simulations performed.

VI. CONCLUSIONS

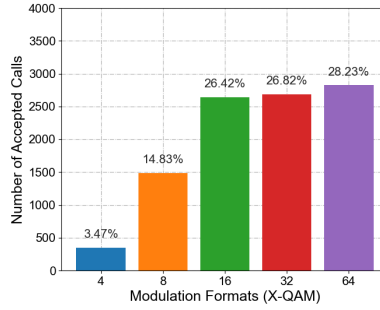
In this paper, we analyzed the impact of wavelength-dependent physical impairments, specifically the optical fiber attenuation coefficient and the optical amplifiers noise figure, considering S, C and L bands in a multiband elastic optical network. Three simulation scenarios were analyzed. The first considered the network performance in which both α and NF had fixed values. The second considered the performance of the network in which α and/or NF could be dependent on the wavelength, considering the transmission in G652.A optical fiber. Finally, the third considered the same aspects as the second, however, the G652.D optical fiber was used.

Table VI: Results of CS3 scenario, in terms of calls blocking probability, considering the network load value equal to 1200 Erlangs for S band, 500 Erlangs for C band and 600 Erlangs for L band.

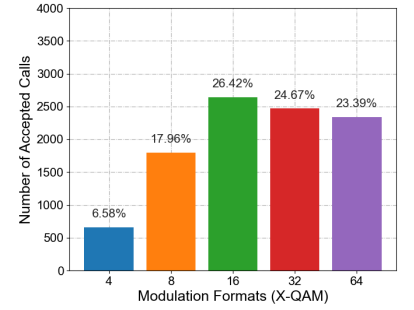
α (dB/km)	S band		α (dB/km)	C band		α (dB/km)	L band	
	NF (dB)	PB		NF (dB)	PB		NF (dB)	PB
0.220	7.0	2.04×10^{-2}	0.191	5.5	4.21×10^{-4}	0.200	6.0	3.57×10^{-3}
0.220	NF(λ)	1.53×10^{-2}	0.191	NF(λ)	2.18×10^{-5}	0.200	NF(λ)	2.71×10^{-4}
$\alpha(\lambda)$	NF(λ)	7.48×10^{-3}	$\alpha(\lambda)$	NF(λ)	1.85×10^{-5}	$\alpha(\lambda)$	NF(λ)	4.14×10^{-5}
$\alpha(\lambda)$	7.0	8.02×10^{-3}	$\alpha(\lambda)$	5.5	3.32×10^{-4}	$\alpha(\lambda)$	6.0	9.47×10^{-4}



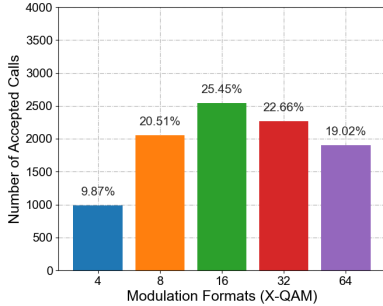
(a) $\alpha = 0,19$ dB/km, $NF = 7$ dB.



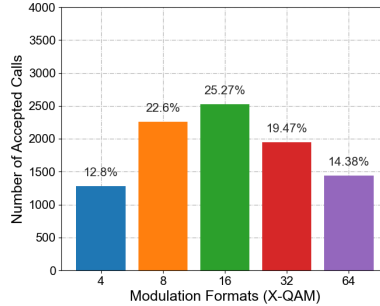
(b) $\alpha = 0,20$ dB/km, $NF = 7$ dB.



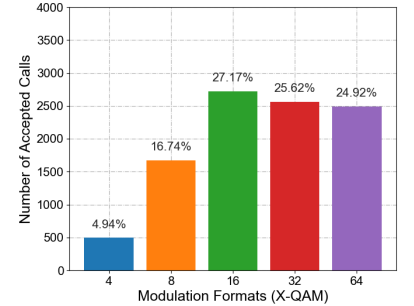
(c) $\alpha = 0,21$ dB/km, $NF = 7$ dB.



(d) $\alpha = 0,22$ dB/km, $NF = 7$ dB.



(e) $\alpha_{G652.A}(\lambda)$, $NF(\lambda)$.



(f) $\alpha_{G652.D}(\lambda)$, $NF(\lambda)$.

Figure 7: Distribution of assigned modulation formats to the network accepted calls, considering S band transmission, a network load value equal to 1200 Erlangs and different scenarios for α and NF : (a) $\alpha = 0,19$ dB/km, $NF = 7$ dB; (b) $\alpha = 0,20$ dB/km, $NF = 7$ dB; (c) $\alpha = 0,21$ dB/km, $NF = 7$ dB; (d) $\alpha = 0,22$ dB/km, $NF = 7$ dB; (e) $\alpha_{G652.A}(\lambda)$, $NF(\lambda)$; (f) $\alpha_{G652.D}(\lambda)$, $NF(\lambda)$.

Table VII: Distribution, in terms of percentage, of assigned modulation formats to the network accepted calls, considering a network load value equal to 1200 Erlangs in S band.

α (dB/km)	NF (dB)	4-QAM (%)	8-QAM (%)	16-QAM (%)	32-QAM (%)	64-QAM (%)
0.19	7.0	0.71	11.82	25.41	28.35	33.68
0.20	7.0	3.47	14.83	26.42	26.82	28.23
0.21	7.0	6.58	17.96	26.42	24.67	23.39
0.22	7.0	9.87	20.51	25.45	22.66	19.02
$\alpha_{G652.A}(\lambda)$	$NF(\lambda)$	12.80	22.60	25.27	19.47	14.38
$\alpha_{G652.D}(\lambda)$	$NF(\lambda)$	4.94	16.74	27.17	25.62	24.92

Table VIII: Distribution, in terms of percentage, of assigned modulation formats to the network accepted calls, considering a network load value equal to 500 Erlangs in C band.

α (dB/km)	NF (dB)	4-QAM (%)	8-QAM (%)	16-QAM (%)	32-QAM (%)	64-QAM (%)
0.19	5.5	1.92	13.08	25.98	27.65	31.36
0.20	5.5	4.76	16.41	26.74	26.00	25.96
0.21	5.5	8.46	19.54	26.36	23.58	21.44
0.22	5.5	11.50	21.46	25.41	21.59	17.26
$\alpha_{G652.A}(\lambda)$	$NF(\lambda)$	1.59	12.71	25.86	27.65	32.19
$\alpha_{G652.D}(\lambda)$	$NF(\lambda)$	0.00	5.04	20.97	30.15	43.84

For the first scenario, we observed that the greater the attenuation value, the greater the value of the total ASE noise power, making the value of $OSNR_{out}$ smaller, affecting the establishment of call requests due to the lack of QoT.

For the second scenario, in which the G652.A optical fiber

was used for the transmission of optical signals, we observed that, for S band, the best performance in terms of calls blocking probability was obtained with $\alpha = 0.220$ dB/km and $NF(\lambda)$. In a more realistic scenario, involving $\alpha(\lambda)$ and $NF(\lambda)$, it resulted in a worse performance due to the fact that

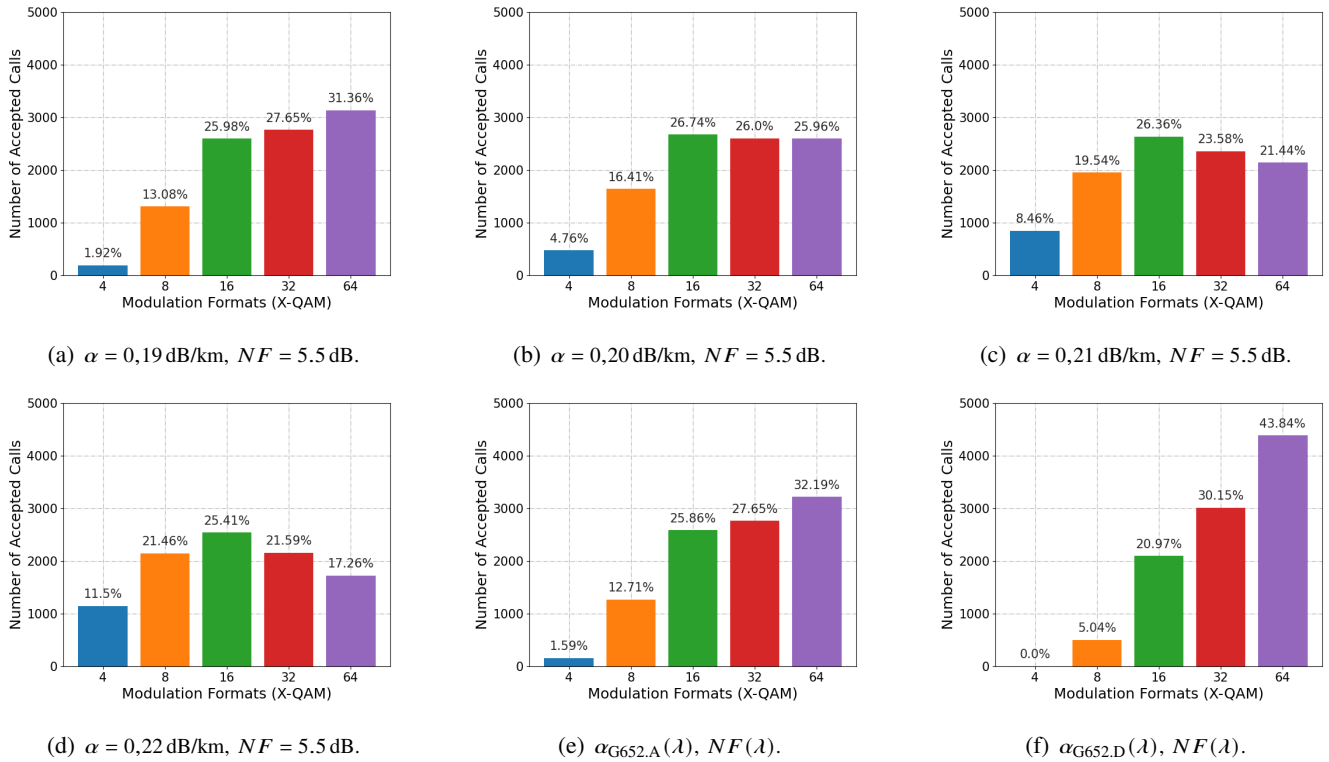


Figure 8: Distribution of assigned modulation formats to the network accepted calls, considering C band transmission, a network load value equal to 500 Erlangs and different scenarios for α and NF : (a) $\alpha = 0.19$ dB/km, $NF = 5.5$ dB; (b) $\alpha = 0.20$ dB/km, $NF = 5.5$ dB; (c) $\alpha = 0.21$ dB/km, $NF = 5.5$ dB; (d) $\alpha = 0.22$ dB/km, $NF = 5.5$ dB; (e) $\alpha_{G652.A}(\lambda)$, $NF(\lambda)$; (f) $\alpha_{G652.D}(\lambda)$, $NF(\lambda)$.

Table IX: Distribution, in terms of percentage, of assigned modulation formats to the network accepted calls, considering a network load value equal to 600 Erlangs in L band.

α (dB/km)	NF (dB)	4-QAM (%)	8-QAM (%)	16-QAM (%)	32-QAM (%)	64-QAM (%)
0.19	6.0	3.42	14.92	26.45	26.93	28.45
0.20	6.0	6.71	18.32	26.49	24.74	23.43
0.21	6.0	10.24	21.03	25.62	22.72	18.97
0.22	6.0	13.13	22.40	24.81	19.92	15.35
$\alpha_{G652.A}(\lambda)$	$NF(\lambda)$	5.68	17.11	26.93	25.21	24.90
$\alpha_{G652.D}(\lambda)$	$NF(\lambda)$	0.05	9.55	24.44	29.21	36.75

the average value of α was above of α fixed value used in the simulations. In the case of C and L bands, the best performance obtained by α with fixed value and $NF(\lambda)$ configuration underestimated the more realistic scenario ($\alpha(\lambda)$ and $NF(\lambda)$).

For the third scenario, in which the G652.D optical fiber was used for the transmission of optical signals, we observed that the configurations that considered $\alpha(\lambda)$ resulted in the best performance in terms of calls blocking probability. This can be explained by the fact that the average value of α was below of the α with fixed value considered in the simulations, resulting in a smaller amount of total ASE noise power at the receiver node and resulting in a smaller calls blocking probability due to the lack of QoT. The performance of the most realistic scenario, in terms of calls blocking probability reduction, compared to the scenario most used in the literature (α and

NF with fixed values) [21], [23] was of approximately 63.41% for S band, 95.60% for C band and 98.84 for L band.

A better distribution of accepted call requests in more efficient modulation formats was observed in the G652.D optical fiber, since the QoT degradation was smaller. The results for C band present the better usability of more efficient modulation formats, culminating in the best utilization values of all scenarios evaluated in this paper (0.00% for 4-QAM, 5.04% for 8-QAM, 20.97% for 16-QAM, 30.15% for 32-QAM, and 43.84% for 64-QAM).

REFERENCES

- [1] R. Ramaswami, K. Sivarajan, and G. Sasaki, *Optical Networks: A Practical Perspective*, 3rd. San Francisco, CA, USA: Morgan Kaufmann Publishers Inc., 2009, ISBN: 978-0-12-374092-2.
- [2] B. C. Chatterjee, N. Sarma, and E. Oki, "Routing and spectrum allocation in elastic optical networks: A tutorial," *IEEE Communications Surveys & Tutorials*, vol. 17, no. 3, pp. 1776–1800, 2015. DOI: 10.1109/COMST.2015.2431731.
- [3] M. Klinkowski, P. Lechowicz, and K. Walkowiak, "Survey of resource allocation schemes and algorithms in spectrally-spatially flexible optical networking," *Optical Switching and Networking*, vol. 27, pp. 58–78, 2018. DOI: 10.1016/j.osn.2017.08.003.

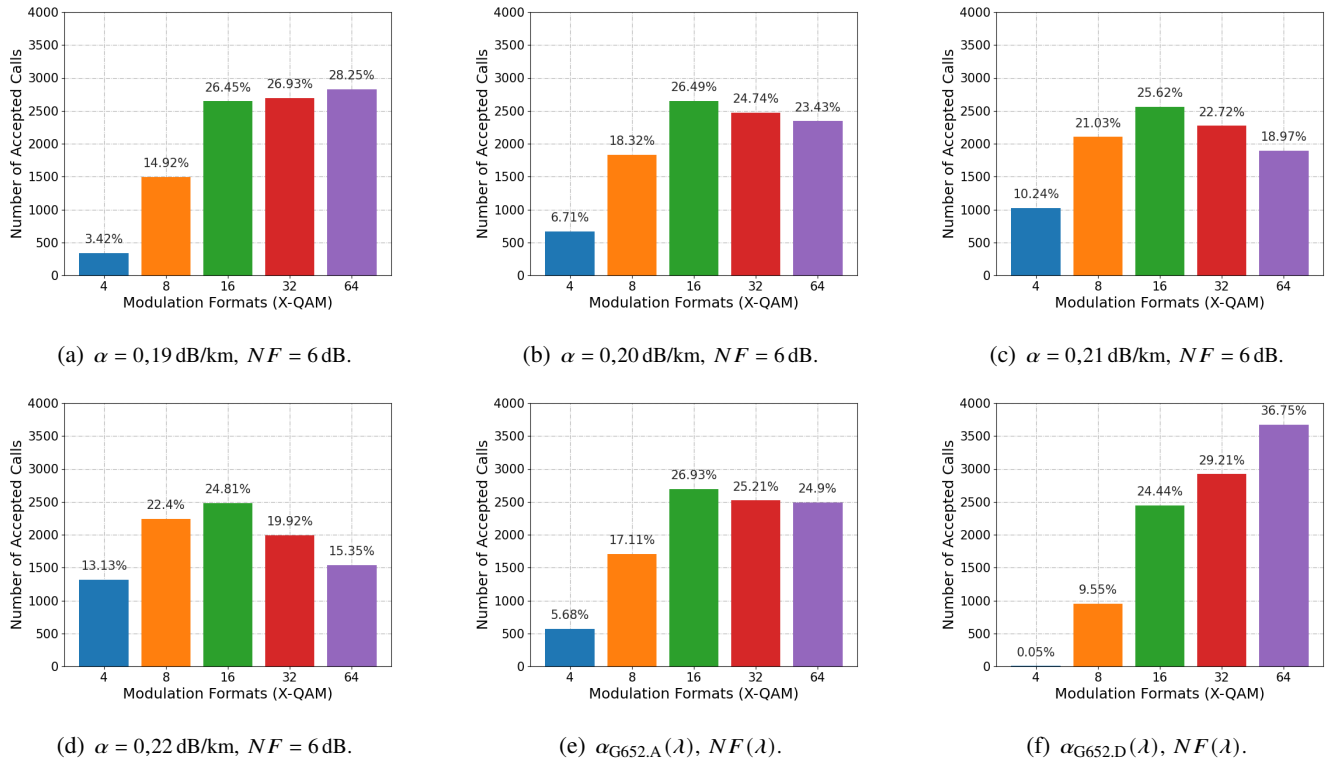


Figure 9: Distribution of assigned modulation formats to the network accepted calls, considering L band transmission, a network load value equal to 600 Erlangs and different scenarios for α and NF : (a) $\alpha = 0,19$ dB/km, $NF = 6$ dB; (b) $\alpha = 0,20$ dB/km, $NF = 6$ dB; (c) $\alpha = 0,21$ dB/km, $NF = 6$ dB; (d) $\alpha = 0,22$ dB/km, $NF = 6$ dB; (e) $\alpha_{G652.A}(\lambda)$, $NF(\lambda)$; (f) $\alpha_{G652.D}(\lambda)$, $NF(\lambda)$.

[4] B. Shariati, J. M. Rivas-Moscoso, D. Klonidis, I. Tomkos, S. Ben-Ezra, F. Jiménez, D. M. Marom, P. S. Khodashenas, J. Comellas, and L. Velasco, "Options for cost-effective capacity upgrades in backbone optical networks," in *European Conference on Networks and Optical Communications (NOC)*, IEEE, 2016, pp. 35–40. DOI: 10.1109/NOC.2016.7506982.

[5] A. Ferrari, A. Napoli, J. K. Fischer, N. Costa, A. D'Amico, J. Pedro, W. Forsyiaak, E. Pincemin, A. Lord, A. Stavdas, J. P. F.-P. Gimenez, G. Roelkens, N. Calabretta, S. Abrate, B. Sommerkorn-Krombholz, and V. Curri, "Assessment on the achievable throughput of multi-band optical transmission systems," *Journal of Lightwave Technology*, vol. 38, no. 16, pp. 4279–4291, 2020. DOI: 10.1109/JLT.2020.2989620.

[6] N. Sambo, A. Ferrari, A. Napoli, N. Costa, J. Pedro, B. Sommerkorn-Krombholz, P. Castoldi, and V. Curri, "Provisioning in multi-band optical networks," *Journal of Lightwave Technology*, vol. 38, no. 9, pp. 2598–2605, 2020. DOI: 10.1109/JLT.2020.2983227.

[7] A. A. Santos-Júnior, H. A. Pereira, and R. C. A. Almeida-Júnior, "Análise do impacto de penalidades físicas na banda c para uma rede óptica elástica," in *XL Simpósio Brasileiro de Telecomunicações e Processamento de Sinais*, vol. 1, 2022, pp. 1–5. DOI: 10.14209/sbirt.2022.1570817480.

[8] N. Sambo, A. Ferrari, A. Napoli, N. Costa, J. Pedro, B. Sommerkorn-Krombholz, P. Castoldi, and V. Curri, "Provisioning in multi-band optical networks: A c+l+s-band use case," in *European Conference on Optical Communication (ECOC)*, 2019, pp. 1–4. DOI: 10.1049/cp.2019.0787.

[9] N. Sambo, A. Ferrari, A. Napoli, N. Costa, J. Pedro, B. Sommerkorn-Krombholz, P. Castoldi, and V. Curri, "Beyond c-band in optical networks," in *International Conference on Transparent Optical Networks (ICTON)*, 2020, pp. 1–4. DOI: 10.1109/ICTON51198.2020.9203488.

[10] M. Nakagawa, H. Kawahara, T. Seki, and T. Miyamura, "Adaptive link-by-link band allocation: A novel adaptation scheme in multi-band optical networks," in *International Conference on Optical Network Design and Modeling (ONDM)*, IEEE, 2021, pp. 1–6. DOI: 10.23919/ONDM51796.2021.9492502.

[11] D. Uzunidis, E. Kosmatos, C. Matrakidis, A. Stavdas, and A. Lord, "Strategies for upgrading an operator's backbone network beyond the c-band: Towards multi-band optical networks," *IEEE Photonics Journal*, vol. 13, no. 2, pp. 1–18, 2021. DOI: 10.1109/JPHOT.2021.3054849.

[12] R. Sadeghi, B. Correia, A. Souza, N. Costa, J. Pedro, A. Napoli, and V. Curri, "Transparent vs translucent multi-band optical networking: Capacity and energy analyses," *Journal of Lightwave Technology*, vol. 40, no. 11, pp. 3486–3498, 2022. DOI: 10.1109/JLT.2022.3167908.

- [13] E. Paz and G. Saavedra, "Maximum transmission reach for optical signals in elastic optical networks employing band division multiplexing," *arXiv preprint arXiv:2011.03671*, 2020.
- [14] F. Calderón, A. Lozada, P. Morales, D. Bórquez-Paredes, N. Jara, R. Olivares, G. Saavedra, A. Beghelli, and A. Leiva, "Heuristic approaches for dynamic provisioning in multi-band elastic optical networks," *IEEE Communications Letters*, vol. 26, no. 2, pp. 379–383, 2021. DOI: 10.1109/LCOMM.2021.3132054.
- [15] P. Morales, P. Franco, A. Lozada, N. Jara, F. Calderón, J. Pinto-Rios, and A. Leiva, "Multi-band environments for optical reinforcement learning gym for resource allocation in elastic optical networks," in *International Conference on Optical Network Design and Modeling (ONDM)*, IEEE, 2021, pp. 1–6. DOI: 10.23919/ONDM51796.2021.9492435.
- [16] N. E. D. El Sheikh, E. Paz, J. Pinto, and A. Beghelli, "Multi-band provisioning in dynamic elastic optical networks: A comparative study of a heuristic and a deep reinforcement learning approach," in *International Conference on Optical Network Design and Modeling (ONDM)*, IEEE, 2021, pp. 1–3. DOI: 10.23919/ONDM51796.2021.9492334.
- [17] D. Uzunidis, F. Apostolopoulou, G. Pagiatakis, and A. Stavdas, "Analysis of available components and performance estimation of optical multi-band systems," *Eng*, vol. 2, no. 4, pp. 531–543, 2021. DOI: 10.3390/eng2040034.
- [18] M. Cantono, A. Ferrari, D. Pileri, E. Virgillito, J. Augé, and V. Curri, "Physical layer performance of multi-band optical line systems using raman amplification," *Journal of Optical Communications and Networking*, vol. 11, no. 1, A103–A110, 2019. DOI: 10.1364/JOCN.11.00A103.
- [19] A. Ferrari, A. Napoli, N. Costa, J. K. Fischer, J. Pedro, W. Forsyiaak, A. Richter, E. Pincemin, and V. Curri, "Multi-band optical systems to enable ultra-high speed transmissions," in *The European Conference on Lasers and Electro-Optics*, Optica Publishing Group, 2019, ci_2_3. DOI: 10.1109/CLEOE-EQEC.2019.8872247.
- [20] A. D'Amico, E. London, E. Virgillito, A. Napoli, and V. Curri, "Inter-band gsnr degradations and leading impairments in c+l band 400g transmission," in *International Conference on Optical Network Design and Modeling (ONDM)*, IEEE, 2021, pp. 1–3. DOI: 10.23919/ONDM51796.2021.9492485.
- [21] K.-F. Nikolaou, D. Uzunidis, A. Stavdas, and G. Pagiatakis, "Quantifying the impact of physical layer effects in an optical multi-band system," in *Telecommunications Forum (TELFOR)*, IEEE, 2021, pp. 1–4. DOI: 10.1109/TELFOR52709.2021.9653339.
- [22] A. D'Amico, B. Correia, E. London, E. Virgillito, G. Borraccini, A. Napoli, and V. Curri, "Scalable and disaggregated ggn approximation applied to a c+l+s optical network," *Journal of Lightwave Technology*, vol. 40, no. 11, pp. 3499–3511, 2022. DOI: 10.1109/JLT.2022.3162134.
- [23] F. Gomes, L. G. Cancela, and J. L. Rebola, "Impact of physical layer impairments on c+l-band metro networks," in *International Conference on Photonics, Optics and Laser Technology (PHOTOPTICS)*, SCITEPRESS—Science and Technology Publications, Lda, 2022, pp. 134–143. DOI: 10.5220/0010909900003121.
- [24] D. Simeonidou, N. Amaya, and G. Zervas, "Infrastructure and architectures on demand for flexible and elastic optical networks," in *European Conference and Exhibition on Optical Communication*, Optica Publishing Group, 2012, Tu.3.D.1. DOI: 10.1364/ECEOC.2012.Tu.3.D.1.
- [25] D. A. A. Mello, A. N. Barreto, T. C. Lima, P. T. F., L. Beygi, and J. M. Kahn, "Optical networking with variable-code-rate transceivers," *Journal of Lightwave Technology*, vol. 32, no. 2, pp. 257–266, 2014. DOI: 10.1109/JLT.2013.2292298.
- [26] *Optical fiber attenuation*, <https://www.fiberoptics4sale.com/blogs/archive-posts/95052294-optical-fiber-attenuation>, Accessed: 2022-02-07.
- [27] B. Correia, R. Sadeghi, E. Virgillito, A. Napoli, N. Costa, J. Pedro, and V. Curri, "Networking performance of power optimized c+l+s multiband transmission," in *IEEE Global Communications Conference (GLOBECOM)*, 2020, pp. 1–6. DOI: 10.1109/GLOBECOM42002.2020.9322068.
- [28] B. Correia, R. Sadeghi, E. Virgillito, A. Napoli, N. Costa, J. Pedro, and V. Curri, "Power control strategies and network performance assessment for c+l+s multi-band optical transport," *Journal of Optical Communications and Networking*, vol. 13, no. 7, pp. 147–157, 2021. DOI: 10.1364/JOCN.419293.
- [29] M. A. Cavalcante, H. A. Pereira, D. A. R. Chaves, and R. C. Almeida-Júnior, "Análise do impacto do ruído ASE em redes ópticas elásticas transparentes usando múltiplos formatos de modulação," in *XXXIII Simpósio Brasileiro de Telecomunicações*, vol. 1, 2015, pp. 1–5. DOI: 10.14209/sbrt.2015.95.
- [30] R. Essiambre, G. Kramer, P. J. Winzer, G. J. Foschini, and B. Goebel, "Capacity limits of optical fiber networks," *Journal of Lightwave Technology*, vol. 28, no. 4, pp. 662–701, February 2010. DOI: 10.1109/JLT.2009.2039464.
- [31] A. Ferrari, E. Virgillito, and V. Curri, "Band-division vs. space-division multiplexing: A network performance statistical assessment," *Journal of Lightwave Technology*, vol. 38, no. 5, pp. 1041–1049, 2020. DOI: 10.1109/JLT.2020.2970484.
- [32] E. B. Sarmento, G. B. Guerra-Júnior, M. G. Costa, I. M. A. Santos, H. A. Pereira, and R. C. A. Almeida-Júnior, "SONDA: Simulador em python para redes ópticas," in *X Conferência Nacional em Comunicações, Redes e Segurança da Informação (ENCOM)*, IECOM, 2020, pp. 1–2.
- [33] G. B. Guerra-Júnior, E. B. Sarmento, M. G. Costa, and H. A. Pereira, "Simulador de código livre aplicado em redes ópticas com multiplexação por divisão espacial,"

in *XXXIX Simpósio Brasileiro de Telecomunicações e Processamento de Sinais*, 2021, pp. 1–5. DOI: 10.14209/sbrt.2021.1570726248.



Ademar Alves dos Santos-Júnior is an undergraduate student in Electrical Engineering at the Federal University of Campina Grande (UFCG). He was a member of the Laboratory of Computacional Modeling of Electromagnetic Effects (LMC2E), during which time he worked in the field of optical networks, specifically with multiband optical transmissions and physical layer impairments. He is currently a member of the Laboratory of Industrial Electronics and Machine Drives (LEIAM). ORCID ID: 0009-0002-3232-5910.



José Roberto do Nascimento Arcanjo was born in Araruna, Paraíba, Brazil, in 1996. He is currently an undergraduate student in Electrical Engineering at the Federal University of Campina Grande (UFCG). He is a member of the Laboratory of Computational Modeling of Electromagnetic Effects (LMC2E). His area of study refers to optical networks, particularly elastic optical networks and multiband optical transmission. ORCID ID: 0009-0007-2258-5918.



Helder Alves Pereira was born in Paulista, Brazil, in 1980. He received the B.Sc. degree in Electronics Engineering from University of Pernambuco (UPE), Recife, Brazil, in 2000. The M.Sc. degree at Telecommunication National Institute (Inatel), Santa Rita do Sapucaí, Brazil, in 2002. The Ph.D. degree in Electrical Engineering at the Federal University of Pernambuco (UFPE), Recife, Brazil, in 2007. He is a Professor at the Electrical Engineering Department of Federal University of Campina Grande (UAEE-UFCG). His interests are related to

fiber optics and optical communications, diffraction and gratings, optics and surfaces, medical optics and biotechnology. ORCID ID: 0000-0003-4232-9317.



Raul Camelo de Andrade Almeida-Júnior has B.Sc. in Electronics Engineering from the Federal University of Pernambuco (1999) and M.Sc. (2001) and Ph.D. (2004) in Electrical Engineering from UNICAMP. Between 2006 and 2011 he worked for the University of Essex, UK, as a Senior Research Officer and in 2012 he joined the Photonics Group, Department of Electronics and Systems of UFPE, in Recife – Brazil, where is currently an Associate Professor. Raul C. Almeida Jr. has experience in Electrical Engineering, focusing on

Telecommunication Systems, and his main interests are in optical networks, traffic engineering, telecommunication networks optimization and projects, analytical modeling, mathematical programming, evolutionary computation, future Internet, machine learning and reinforcement learning. ORCID ID: 0000-0003-2047-7167.